J. Phys. D: Appl. Phys. 58 (2025) 475101 (9pp)

Effect of buffer layer thickness on recombination in zincblende InGaN/GaN quantum wells

X Xu^{1,*}, D Dyer², M Frentrup¹, W R Fieldhouse-Allen², M J Kappers¹, G Kusch¹, D J Wallis^{1,3}, R A Oliver¹, and D J Binks²

E-mail: xx838@cam.ac.uk

Received 12 August 2025, revised 5 November 2025 Accepted for publication 10 November 2025 Published 18 November 2025



Abstract

InGaN/GaN quantum wells grown in the zincblende phase along the [001] direction are free of the internal electric fields that reduce the radiative recombination rate in conventional quantum wells grown along the *c*-axis in the wurtzite phase. However, heteroepitaxial growth and reduced thermodynamic stability compared to the wurtzite phase typically results in a significant density of stacking faults (SFs) in zincblende GaN, which impacts emission efficiency when they intersect quantum wells. Here it is shown that increasing the buffer layer thickness that lies between the substrate and the active region significantly reduces the density of SFs reaching the quantum well, and thereby increases the emission efficiency.

Supplementary material for this article is available online

Keywords: zincblende gallium nitride, cathodoluminescence, photoluminescence, stacking faults, light emitting diodes

1. Introduction

Current light-emitting diode (LED) technology for lighting applications typically utilises c-plane wurtzite (wz) InGaN/GaN quantum wells (QWs). However, the use of this crystal phase and growth direction produces an internal electric field on the order of MV cm⁻¹ across the QWs, which acts

Original content from this work may be used under the terms of the Creative Commons Attribution 4.0 licence. Any further distribution of this work must maintain attribution to the author(s) and the title of the work, journal citation and DOI.

to separate electrons and holes [1]. Such an increased separation reduces the rate of radiative recombination in the QW, impacting the internal quantum efficiency of the LED. For blue-emitting LEDs, this effect can be mitigated by decreasing the QW thickness, allowing wall plug efficiencies of 84% to be achieved in spite of these internal fields [2]. However, the strength of the internal field increases with higher indium content, reducing the radiative recombination rate further. The negative impact of this on the efficiency of devices emitting at longer wavelengths is potentially exacerbated by other issues associated with higher indium content, such as increased alloy fluctuations [3] and an increased density of trench defects [4]. Consequently, c-plane wz LEDs emitting in the green and amber spectral regions exhibit efficiencies that are significantly less than for their blue counterparts [3].

¹ Department of Materials Science and Metallurgy, University of Cambridge, Cambridge CB3 0FS, United Kingdom

² Department of Physics and Astronomy & Photon Science Institute, University of Manchester, Manchester M13 9PL, United Kingdom

³ Centre for High frequency Engineering, Cardiff University, Cardiff CF24 3AA, United Kingdom

^{*} Author to whom any correspondence should be addressed.

The challenges associated with achieveing efficient emission from wz c-plane LEDs emitting at longer wavelengths have motivated the study of alternative growth directions of the wz-phase that eliminate or reduce the internal field across the QW [5]. Another promising approach is to grow the LED structure in the zincblende (zb) rather than the wz phase of GaN. When grown along the [001] direction, zb QWs are completely free of the internal fields [6], resulting in sub-ns recombination lifetimes [7, 8] i.e. two orders of magnitude smaller than for similar c-plane wz QWs [9]. A further advantage of zb-GaN is that its bandgap (3.3 eV at low temperature [10]) is significantly less than that of wz-GaN (3.5 eV at low temperature [10]) so that less indium incorporation is required for long wavelength emission. However, whilst zb GaN-based LEDs have been reported, there efficiency currently lags behind that of their wz counterparts [11]. Hence, studies to understand the impacts of materials growth and structure on device performance are still required.

Heteroepitaxial growth of zb-GaN onto substrates such as 3 C-SiC/Si (3.4% lattice mismatch [12]) results in the formation of a considerable density of stacking faults (SFs) i.e. wz monolayers within the zb lattice [13]. The prevalence of SFs is attributed to the greater thermodynamic stability of the wz phase [14, 15] and to the dissociation of perfect dislocations into energetically preferred partial dislocations at the interface with the substrate [16]. Several recent studies have indicated that the SFs have an important role in determining the emission properties of zb-QWs. Significant indium segregation has been found adjacent to SFs [17], which increases the spectral breadth of the emission from zb-QWs [7]. SFs also appear as darker regions in cathodoluminescence (CL) studies of the microstructure of zb-QWs [18] suggesting that they reduce emission efficiency.

In this work, the effect of buffer layer thickness, t_B , on the SF density and on the recombination in the QW is investigated. Earlier work by Vacek *et al.* suggests that as the zb GaN layer thickness increases, SFs on different {111} planes can eventually meet so that their Burgers vector may react so that the SFs annhilate each other [16]. This is further supported in the simulations of Lee *et al.*, which showed that, in theory, a substantial decrease in the density of SFs can be achieved by using thick buffer layers [13]. Here, we show experiemntally that increasing t_B to 1.5 μ m or greater significantly reduces the number of SFs that intersect with the QW and that this results in increased emission efficiency.

2. Methods

2.1. Sample growth

The samples analysed in this study were grown using metalorganic vapour-phase epitaxy on 3 C-SiC/Si (001) substrates with a 4° miscut towards the [1–10] direction, employing an Aixtron 6×2 in. CCS reactor. Three series of samples were studied, as illustrated in figure 1. Series 1 comprises a set of samples with a thin 44 nm thick nucleation layer followed by a single GaN buffer layer of varying thickness. Four samples with buffer layer thicknesses of $t_B = 0.6 \,\mu\text{m}$, 1.5 μm , 2.3 μm , and 3.0 μ m were grown under conditions that had previously been optimised to suppress the formation of unwanted wz-GaN incslusions [19]. Series 2 is based on a similar set of buffer layers with thicknesses between 0.6 μ m and 3.0 μ m. These were overgrown together in one growth run with an additional 200 nm of non-intentionally doped GaN, so that the total GaN buffer layer thicknesses, $t_{\rm B}$, were 0.8 μ m, 1.1 μ m, 1.4 μ m, $1.7 \mu m$, $2.5 \mu m$, and $3.2 \mu m$, respectively. This was followed by the growth of a 2.3 nm wide $In_xGa_{1-x}N$ single quantum well (SQW) at a temperature of around 720 °C, which was capped with an 11 nm thick GaN layer. The QW thickness of 2.3 nm was chosen to provide structures comparable with typical c-plane wz structures, with thicknesses in the 2 nm to 3 nm range [20]. Finally, in Series 3 a multiple quantum well (MQW) structure was grown on a set of GaN buffer layers with total thicknesses of $t_B = 0.8 \mu \text{m}$, 1.7 μm , 2.5 μm , and 3.2 μ m, respectively. In this series, an additional 4 nm thick $In_rGa_{1-r}N$ underlayer ($x \approx 1\%$) was included below the first QW. It has been shown for hexagonal c-plane MQWs that such an underlayer improves the overall performance of the MQWs, which makes this heterostructure more device relevant [21]. The MQWs grown on top of this underlayer consist of five InGaN QWs with a nominal width of 2.3 nm, each topped by a 11 nm thick barrier.

2.2. X-ray diffraction (XRD) studies

The samples in Series 1 were studied by XRD to assess the impact of changing layer thickness on the crystal quality. For this purpose, XRD reciprocal space maps were recorded around the 113-type zb-GaN and 1–103 wz-GaN reflections parallel and perpendicular to the miscut direction of the substrate with a PIXcel solid-state area detector in a PANalytical Empyrean diffractometer. Intensity profiles along the SF-streak between the two nearby reflections were then extracted, and subsequently fitted with three Pseudo-Voigt functions to account for the zb and wz reflections, and for an ill-defined diffuse scattering between them thought to be related to highly defective zb regions in the investigated GaN buffer layers. The integrated intensities of these fit profiles were then used to quantify the zb-GaN fraction following the description in [12].

2.3. Cathodoluminescence studies

Series 2 was designed for cathodoluminescence studies. Since in (001)-oriented zb-GaN SFs form on {111} planes, and are thus inclined to the growth direction, SQWs without InGaN underlayer were preferred for this study to avoid confusion in data interpretation arising from the prescence of SF intersections with quantum well or underlayer material located at different depths in the sample. Room temperature CL measurements were conducted with an Attolight Allalin 4027 Chronos scanning electron microscopy-cathodoluminescence (SEM-CL) system, using a 150 l mm⁻¹ grating blazed at 500 nm.

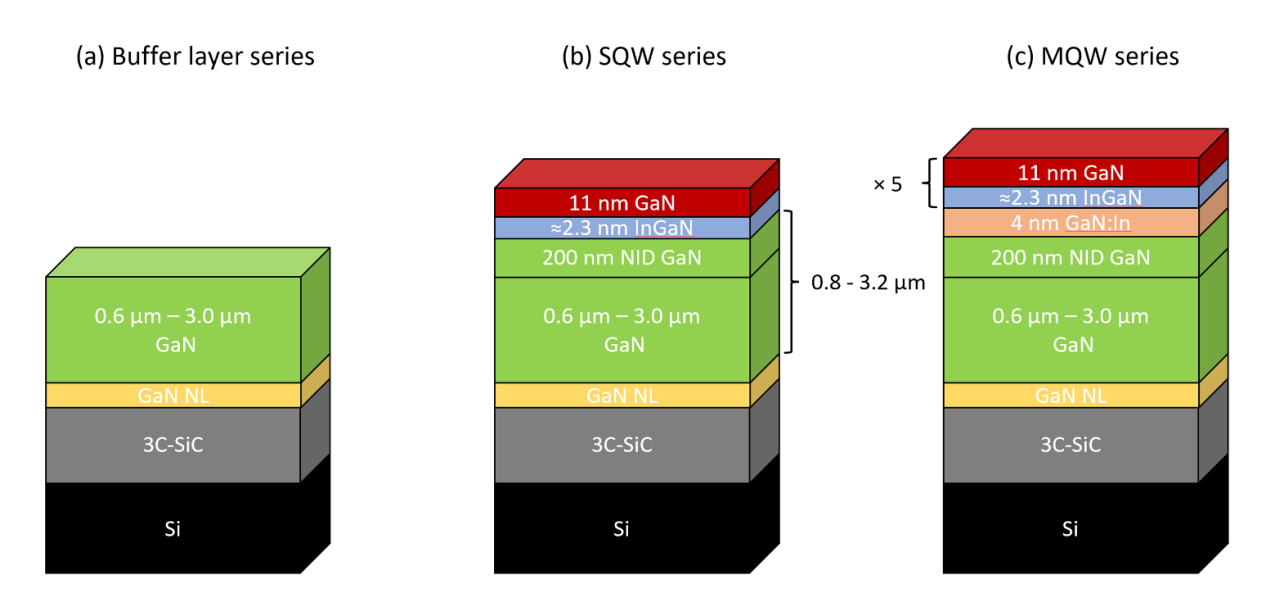


Figure 1. Schematic structures of the three different sets of samples. (a) GaN buffer layers, (b) SQW samples, and (c) MQW structures.

A 5 keV electron beam with an interaction volume reaching approximately 90 nm into the sample, a probe current of 1.25 nA and an aperture size of 50 μ m was used to collect hyperspectral CL maps and concurrent secondary electron (SE) images with a size of 7.56 μ m \times 7.56 μ m and a resolution of 128 pixels \times 128 pixels. In the hyperspectral data sets a full spectrum is associated with each pixel of the map, which allows analysis of spectral differences across the map. For all measurements the dwell time was 100 ms per pixel. The measured CL data were analysed with the open-source python-based LumiSpy package [22].

2.4. Photoluminescence experiments

The MQWs in series 3 were studied by photoluminescence (PL) spectroscopy. Using MQWs for the PL experiment ensure that changes seen in temperature dependent data are not dominated by thermionic emission out of a SQW and introduces into our study a structure relevant to the active region of a device. PL measurements were conducted at 12 K by placing the samples on the cold finger of an evacuated, closed-cycle helium cryostat. For steady-state measurements, the samples were excited above the bandgap of zb-GaN using the 325 nm (3.8 eV) line of a continuous wave 10 mW HeCd laser. The laser was focused onto the sample using a lens with a focal length of 15 cm, resulting in a spot size of 80 μ m. The emitted PL was collected and directed into the entrance slit of a spectrometer with a spectral resolution of 4.8 nm and then detected by a photomultiplier tube (PMT). A mechanical chopper was used to modulate the HeCd laser, and the reference signal from the chopper, along with the PMT signal, was sent to a Stanford Instruments lock-in amplifier for phase-sensitive detection, enhancing the signal-to-noise ratio. Neutral density filters were used to adjust the power density incident on the samples. Statistics on spectrally integrated QW emission intensities were obtained at room temperature using a confocal microscope system to collect light from 14×14 array of regions on each sample, each of which was 75 μ m in diameter. Excitation was through the same microscope and used an ultrafast laser (Light Conversion Pharos PH2-20 W) emitting 260 fs pulses at 1 MHz repetition rate, frequency tripled to obtain an excitation wavelength of 343 nm with an average power density of 10 W·cm⁻²; detection was via a fibre-coupled spectrometer (Horiba iHR 550) and CCD array (Horiba Synapse). PL decay transients were obtained by exciting the samples with 100 fs pulses at a wavelength of 266 nm (4.7 eV) generated by a mode-locked Ti:sapphire laser and up-converted to the third harmonic. The resulting PL transients were found by using a microchannel plate at the exit slit of the spectrometer and employing the time-correlated single photon counting technique.

3. Results

3.1. Series 1: Buffer layers

To investigate the impact of the buffer layer thickness on the crystal quality of the four samples in series 1, a quantitaive phase analysis has been performed by XRD. Figure 2 shows that the zb phase purity across all samples is relatively high and improves from about 94% to above 98% with increasing GaN buffer thickness. This observation is related to the suppression of small amounts of inclusions of the wz phase and defect-rich regions in the samples to a total of less than 2% for the sample with 3.0 μ m buffer thickness (see supplementary material figure S1). This improvement in crystal quality was also supported by room-temperature PL measurements of the near-band edge emission, showing an increase in the maximum intensity by roughly an order of magnitude between the thinnest and

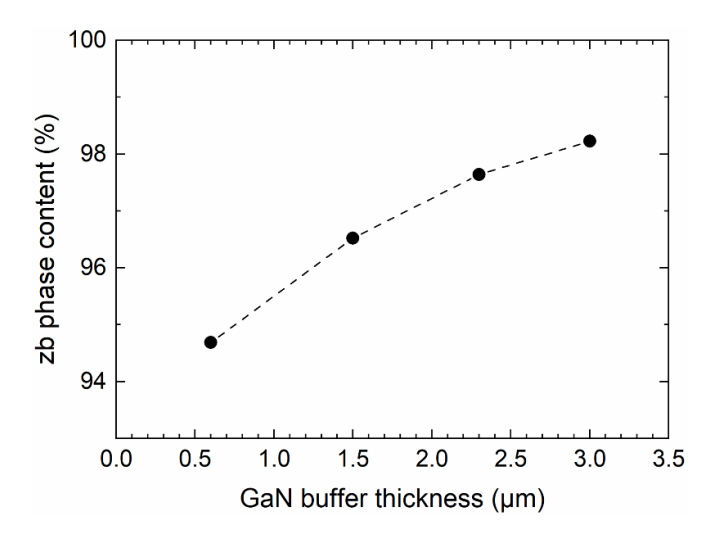


Figure 2. XRD phase analysis of the zb fraction for samples with buffer layer thickness between $0.6~\mu m$ and $3.0~\mu m$.

the thickest buffer layer sample (see supplementary material figure S2).

3.2. Series 2: Single quantum wells

Representive panchromatic CL maps of the six SQW samples are shown in figure 3. All maps show a pattern of rectangular bright patches bounded by a network of low-intensity dark stripes running along the $\langle 110 \rangle$ directions. These dark stripes have previously been suggested to be associated with the agglomeration of non-radiative recombination centres in the vicinity of {111}-type SFs near the sample surface [18]. Across the sample series it appears that the density of dark stripes reduces as the buffer thickness increases. For a statistical analysis of these features, ten parallel lines of equal spacing have been drawn on each of the CL maps for both inplane $\langle 110 \rangle$ directions, respectively, and the number of intersections of these lines with the dark stripes have been evaluated. For each sample, CL maps of three different regions have been analysed to determine an average value and a standard deviation for the density of SF-related dark stripes. Figure 4(a) shows that for both in-plane directions the SF-related dark stripes reduce in density from about $3.0 \times 10^4 \text{ cm}^{-1}$ to about $1.5 \times 10^4 \text{ cm}^{-1}$ as the total thickness of the GaN buffer increases from 0.8 μ m to 3.2 μ m. This implies that the density of SFs reduces with increasing buffer layer thickness, consistent with the reduction of intensity from highly defective material seen in the XRD analysis for the buffer layer samples of series 1 in section 3.1. However, it should be noted that the density of dark stripes gives an underestimation of SF density, because SFs are often present in these samples in bunches [17], and the resolution of the CL measurements is insufficient to observe separate features from each SF within a bunch. One might speculate that broader, darker stripes are more likely to

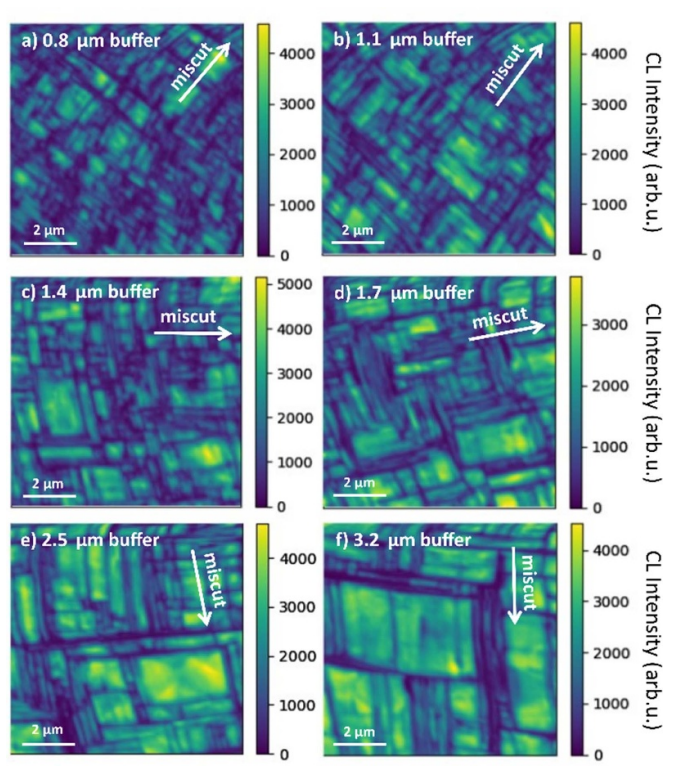
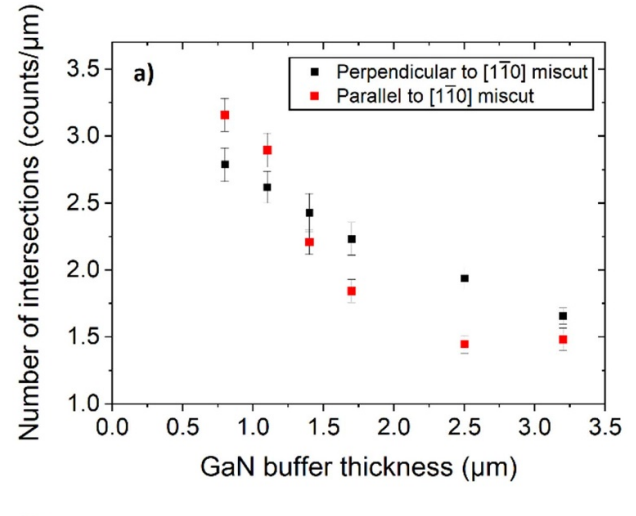


Figure 3. Panchromatic CL maps for the SQW samples with GaN buffer thicknesses of a) $0.8 \mu m$, b) $1.1 \mu m$, c) $1.4 \mu m$, d) $1.7 \mu m$, e) $2.5 \mu m$, f) $3.2 \mu m$. All measurements were performed at 300 K.

relate to SF bunches and narrower, less pronounced stripes to individual SFs.

Compared to the dark stripes, the rectangular patches in the CL maps of the SQW samples in figure 3 are significantly brighter and more homogenous in their light emission, suggesting that these regions relate to low defect density regions with low SF density. As shown in figure 4(b), the mean area of individual bright patches increases significantly from (0.050 \pm 0.002) μm^2 for the SQW grown on the thinnest GaN buffer to (0.365 \pm 0.035) μ m² in the case of the thickest buffer, while in the CL maps of figure 3 the density of bright patches decreases monotonoically as the buffer thickness increases. Both observations are consistent with a reduction of the SF density. Furthermore, the CL emission intensity within the bright patches increases, which might be related to an increasing average distance from the centre of the bright patches to the SFs, reducing the likelihood that free carriers will be able to diffuse to SFs and recombine non-radiatively. In consequence, it becomes more likely that carriers recombine radiatively within the SQW, leading to an overall increase of the intensity from individual patches.

The mean CL spectra across each of the hyperspectral maps for the six SQW samples in series 2 are shown in figure 5. The majority of the light intensity comes from the QW and is emitted at about 2.6 eV, while the zb-GaN near-band-edge



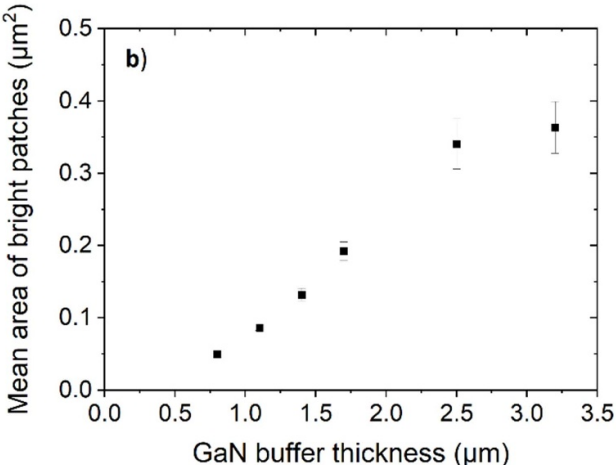


Figure 4. (a) Variation in the density of SF-related dark stripes in CL maps with GaN buffer thickness parallel and perpendicular to the $\begin{bmatrix} 110 \end{bmatrix}$ miscut direction. (b) Mean area per bright patch against buffer thickness.

emission at about 3.2 eV only contributes a small amount to the total intensity. Across the samples, the intensity of QW emission increases as the buffer thickness increases, consistent with an improvement of the crystal quality by reduction of the defect density in the sample, suggested by the previous observations from XRD and our interpretation of the CL maps. Interestingly, the maximum of the QW emission blue shifts slightly by 30-50 meV and the low energy tail of the QW emission peak becomes weaker with increasing buffer thickness (see supplementary material figure S3). This small blue shift is unexpected given that as the buffer layer thickness increases, we observe a slight temperature drop at the surface during the SQW growth for thicker buffer layers, which would be expected to result in a slightly increased indium incorporation into the InGaN QW, and hence a red shift in the emission (see supplementary material figure S4). We hence hypothesise that both the weakening low energy tail and also the blueshift may relate to the reduction in SF density.

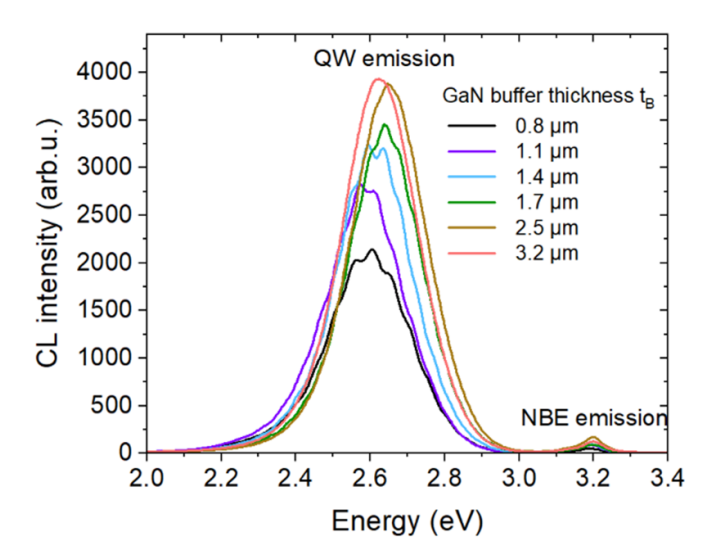


Figure 5. Mean CL spectra of the zb-InGaN SQW samples of series 2. All measurements were performed at 300 K.

To investigate this hypothesis, a band-pass filter between 2.15 eV and 2.25 eV was applied to the CL maps to highlight the intensity distribution of the low energy shoulder of the SQW peak, as shown in figure 6. Bright lines can be observed, which reduce in density with a greater buffer layer thickness and which tend to be located close to (or on) the position of the SF-related dark stripes in the panchromatic CL maps of figure 3. It has previously been reported that the intersection of SFs with an InGaN SQW can lead to the formation of elongated indium-enriched regions [17] which result in quantum wire (Qwire)-like features in the emission spectrum [23]. We would expect that such indium enriched regions will emit at a slightly lower energy than the surrounding SQW, and that the low energy shoulder of the QW emission peak is indeed related to emission from such SF-related indium-enriched material. Interestingly, the vast majority of the bright lines in figure 6 appear to align perpendicular to the [1–10] miscut direction. This is consistent with obersevations by Gundimeda et al on the predominant orientation of Qwire features in a similar SQW sample, which was related to the significantly higher density of SFs intersecting the OWs perpendicular to the miscut than parallel to the miscut [23]. However, here we note that despite there being multiple features associated with SFs parallel to the miscut in the panchromatic images (figure 3), very few of the observed low energy emission features align in this direction, raising the possibility that there are also differences in the segregation occurring to the different orientations of SF.

3.3. Series 3: Multiple quantum wells

The low temperature PL spectra for the four MQW samples in series 3 are compared in figure 7. In each case the emission is dominated by a broad QW peak centred at 2.75 eV with a full width half maximum of \approx 150 meV. The spectra

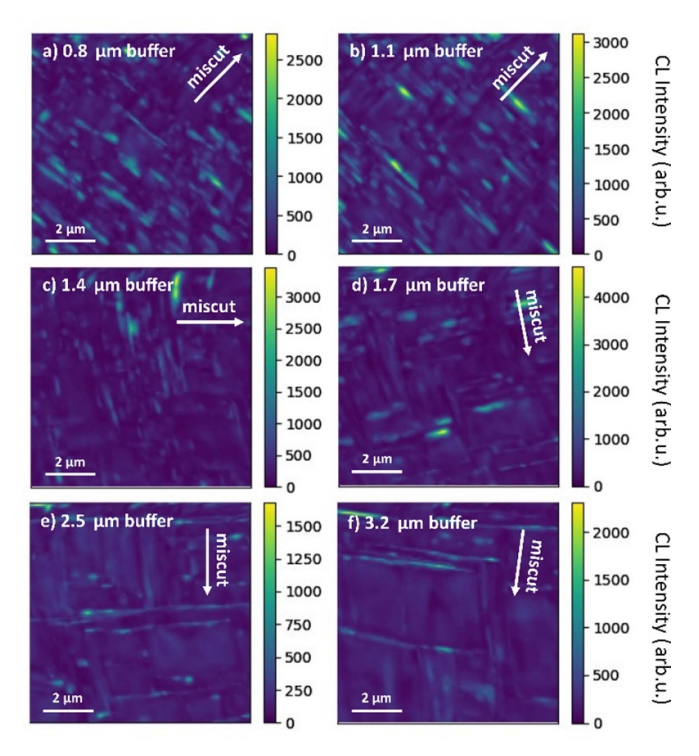


Figure 6. Band-pass filtered (2.15–2.25 eV) CL maps showing the spatial distribution of the CL emission intensity from the low energy shoulders of the SQW peak for the sample with a) 0.8 μ m, b) 1.1 μ m, c) 1.4 μ m, d) 1.7 μ m, e) 2.5 μ m and f) 3.2 μ m zb GaN buffer. All measurements were performed at 300 K.

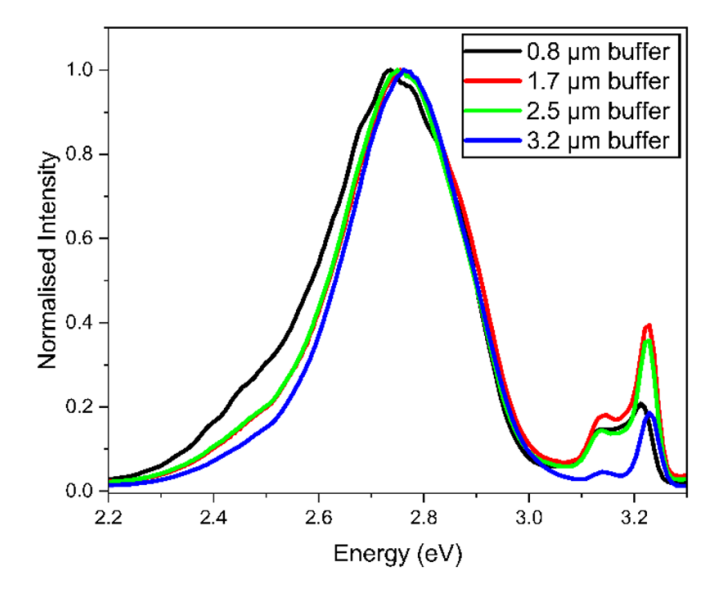


Figure 7. 12 K PL emission spectra for MQW samples with buffer layer thicknesses ranging from 0.8 μ m to 3.2 μ m. The excitation power density used was 10 W·cm⁻².

for each $t_{\rm B}$ value are very similar on their high energy side but differences can be seen on the low energy side, with a shoulder centred at about 2.5 eV being evident which reduces in intensity as $t_{\rm B}$ increases. This is consistent with the observation of a reduced tail at low emission energies in the CL

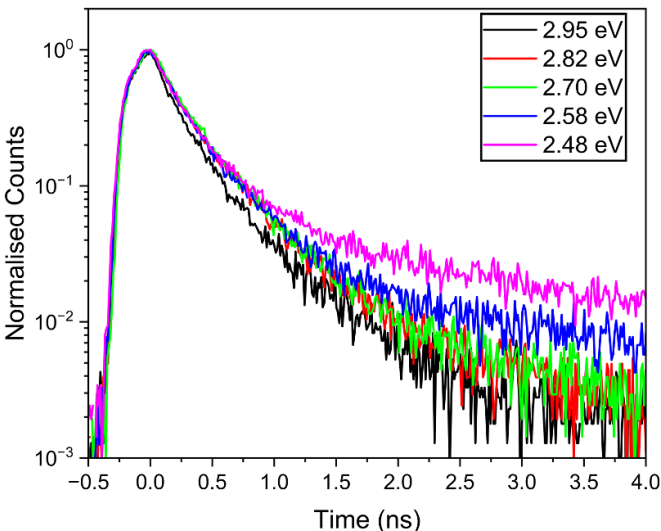


Figure 8. 12 K PL transients for photon energies spanning the emission band for the $t_{\rm B}=3.2~\mu{\rm m}$ sample.

data (figure S3). Given the reduction in SF density noted above for greater t_B , and the fact that the low energy features can be associated with the SFs using the band-pass-filtered CL maps (figure 6), the shoulder observed in PL is likely to be associated with SFs. There are also some near band edge peaks in the 3.1 eV to 3.3 eV region; similar features have been reported previously which were attributed to donor bound exciton and donor-acceptor pair recombination in the GaN [24].

Figure 8 shows the PL decay transients obtained at various emission energies for the $t_B = 3.2 \mu m$ sample; similar data for the other samples are given in the supplementary material (see figure S5). Each transient is very similar for the first 0.5 ns after the initial peak but after that different behaviour is observed. The transients at energies corresponding to the main emission peak (2.70-2.95 eV) remain similar to each other but those at energies corresponding to the low energy shoulder noted in the PL spectra (2.48 eV and 2.58 eV—see figure 7) decay more slowly. This difference in decay behaviour is consistent with the low energy shoulder region being due to emission from a different microstructural feature than the main emission peak. The formation of microstructures that result in Type II confinement of carriers due to the existence of closely-spaced SFs has previously been used to explain the PL spectra observed for cubic GaN epilayers [24]. One possibility is that similar Type II carrier confinement arises in the QWs investigated in this study due to some combination of indium segregation and closely space SFs, reducing the electron-hole wavefunction overlap and thus the recombination rate for that fraction of the carrier population confined by the Type II structures.

The normalised temperature dependence of the spectrally integrated emission spectrum for the 3.2 μ m sample is shown in figure 9. The reduction in emission with increasing temperature is consistent with a greater probability of carriers encountering a non-radiative recombination centre. The relative intensity at 300 K, i.e. its value as a percentage of the

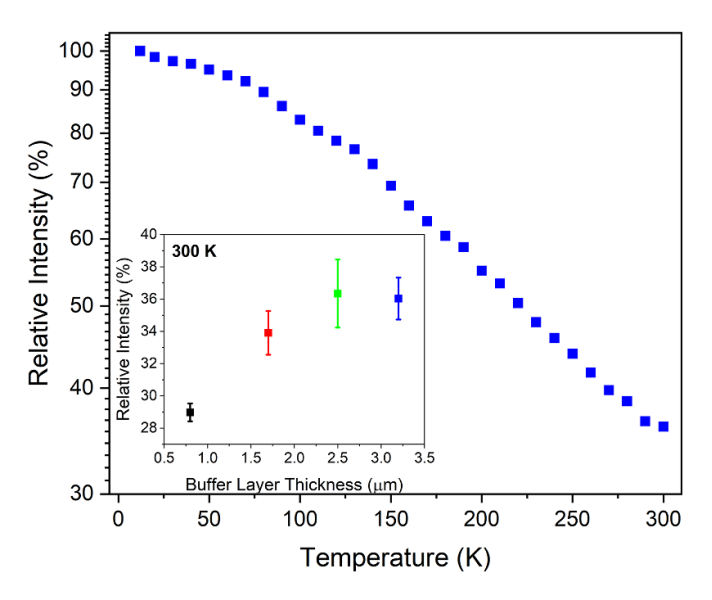


Figure 9. Normalised temperature-dependence of the spectrally integrated emission intensity for the 3.2 μm buffer layer sample. Inset shows the intensity at 300 K relative to the intensity at 12 K for the MQW series as a function of buffer layer thickness. The error bars shown correspond to the standard deviation of 196 room temperature measurements taken over a 14 \times 14 array of adjacent positions across each sample.

intensity at low temperature, as a function of buffer layer thickness for the MQW series is shown in the inset of figure 9. The $t_{\rm B}=0.8~\mu{\rm m}$ sample suffers the greatest loss of emission intensity as the temperature is increased to 300 K, with the intensity reducing to about 29% of its low temperature value. In contrast, the other samples exhibit a smaller loss of intensity with temperature, each reducing to about 34%–36% of their low temperature emission intensity; only minor intensity increases are evident as $t_{\rm B}$ increases beyond 1.7 μ m, as was the case for the CL intensity described above. This suggests that most of the improvement in emission efficiency obtained from a reduction in SFs is achieved by increasing t_B to 1.7 μ m with little additional benefit resulting for further increases in $t_{\rm B}$. This is consistent with the identification of SFs as a key source of non-radiative recombination in zb-QWs for $t_{\rm B}$ up to 1.7 μ m, but after that other sources become more important so increasing t_B has less impact. Various authors have previously used the relative intensity at 300 K as an estimate of the internal quantum efficiency (IQE) of wz-InGaN/GaN QWs [25–27]. This approach assumes that the IQE at low temperature is ~100% because carriers are not sufficiently mobile to encounter non-radiative recombination centres to a significant degree. Notwithstanding this assumption, this method provides a useful means of comparison with the zb-InGaN/GaN QWsreported here. For instance, for a stack of eight 3 nm wide wz-QWs emitting at 2.7 eV Wang et al found by this method that the peak IQE was \sim 65% [25]. More recently Alreshidi et al also used the relative intensity at 300 K to estimate the IQE for stacks of nine 3 nm wz-QWs, also emitting at 2.7 eV, and found that it improved from 40% to nearly 90% as the number of superlattice pairs under the MQWs was increased from 1 to 12 [26]. Thus, using relative intensity we estimate the IQE of these zb-QWs to be typically 2–3 times less than that of comparable wz-QWs.

4. Discussion

Across the three methodologies it can be observed that increasing buffer thickness reduces SF density and this has a signficant impact on carrier recombination in zb-InGaN/GaN QWs. XRD and CL maps indicate an improvement in material quality as buffer thickness is increased. Both the CL and PL emission spectra show suppression of a low energy tail or shoulder within the QW emission band with increasing buffer thickness. The low energy tail is associated with SF regions within the QW layers (see figure 6). Similar features have been reported previously for MOCVD-grown blue-emitting zb-InGaN/GaN QWs [17] and linked to the formation of QWires within the QW layer. The emission from these microstructural features is noted to exhibit decay tails that persist for longer times compared to the rest of the QW emission band [7], as observed in figure 8 of this article.

The improvement in material quality, suppression of SFrelated emission, and increase in QW emission efficiency at 300 K by increasing the buffer layer thickness, is beneficial for realising higher efficiency zb-LEDs. However, due to the anisotropic distribution of SFs [13], there is a limit to the benefit of increasing buffer layer thickness. Above 2.5 μ m in both XRD and CL measurements, very little change can be observed in the zb phase purity or SF density. Consistent with this, no significant improvement in the relative QW intensity at 300 K could be observed as the buffer layer is grown above 1.7 μ m, suggesting that SFs are no longer the most important non-radiative recombination channel for samples with these thicker buffer layers. As noted above, the estimated IQE for these zb-QWs is 2-3 times smaller than for comparable wz-QWs. However, the high IQEs now reported for wz-QWs are the result of a series of improvements made over decades whereas comparatively little effort has been focused on increasing the IQE of zb-QWs to date. There are several approaches that have been successfully used to enhance wz-QW IQE that could be adopted for zb-QWs. For instance, the use of underlayers that are 10 s of nm in thickness has been shown to signficantly reduce the point defect density in the QW region, and thus the associated non-radiative recombination [21, 28]. The strain engineering enabled by varying the number of superlattice numbers underneath the QWs has been shown to improve the IQE, as mentioned above [26].

5. Conclusion

The removal of SFs, the dominant extended defect within the zb-InGaN/GaN QWs, is crucial to achieve efficient zb-LEDs. In this paper, XRD, CL mapping and photoluminescence techniques were used to study the effect of buffer layer thickness on the SF density within zb-InGaN/GaN QWs. By

monitoring both material quality and the emission properties of the QWs, it is observed that increasing the buffer thickness reduces SF density; this improves the zb phase purity, suppresses unwanted SF-related emission within the QW layer and improves the QW emission efficiency at 300 K. However, most of the benefit to materials quality and QW emission efficiency is achieved for a buffer thickness of 1.7 μ m, with less to be gained for thicknesses greater than this.

Data availability statement

The data that support the findings of this study are openly available in the University of Cambridge repository Apollo at https://doi.org/10.17863/CAM.121700.

Acknowledgments

This work was enabled through financial support by the UK Engineering and Physical Sciences Research Council (EPSRC) under the research Grants EP/W03557X/1 and EP/W034956/1, 'Fast Switching Zincblende GaN LEDs'. The CL facility was funded by the EPSRC Grant EP/R025193/1, 'Time-resolved cathodoluminescence scanning electron microscope'.

For the purpose of Open Access, the author has applied a CC BY public copyright license to any Author Accepted Manuscript (AAM) version arising from this submission.

Author contributions

X Xu D 0009-0006-4526-2946

Data curation (equal), Formal analysis (equal), Investigation (lead), Writing – original draft (lead), Writing – review & editing (lead)

D Dyer 0 0000-0003-2097-3689

Data curation (equal), Formal analysis (equal), Investigation (lead), Writing – original draft (lead), Writing – review & editing (lead)

M Frentrup 0000-0002-1726-3099

Data curation (equal), Formal analysis (equal), Investigation (equal), Supervision (equal), Writing – original draft (lead), Writing – review & editing (lead)

W R Fieldhouse-Allen

Data curation (equal), Formal analysis (equal), Investigation (supporting), Writing – original draft (supporting), Writing – review & editing (supporting)

M J Kappers

Investigation (equal), Writing – original draft (supporting), Writing – review & editing (supporting)

G Kusch © 0000-0003-2743-1022

Supervision (equal), Writing – original draft (supporting), Writing – review & editing (supporting)

D J Wallis

Funding acquisition (lead), Project administration (lead), Supervision (equal), Writing – original draft (equal), Writing – review & editing (equal)

R A Oliver 0 0000-0003-0029-3993

Funding acquisition (lead), Project administration (lead), Supervision (lead), Writing – original draft (equal), Writing – review & editing (equal)

D J Binks D 0000-0002-9102-0941

Funding acquisition (lead), Project administration (lead), Supervision (lead), Writing – original draft (equal), Writing – review & editing (equal)

References

- [1] Ren C X 2016 Polarisation fields in III-nitrides: effects and control *Mater. Sci. Technol.* **32** 418–33
- [2] Narukawa Y, Ichikawa M, Sanga D, Sano M and Mukai T 2010 White light emitting diodes with super-high luminous efficacy J. Phys. D: Appl. Phys. 43 354002
- [3] Auf der Maur M, Pecchia A, Penazzi G, Rodrigues W and Di Carlo A 2016 Efficiency drop in green InGaN/GaN light emitting diodes: the role of random alloy fluctuations *Phys. Rev. Lett.* 116 027401
- [4] Massabuau F C-P *et al* 2014 The impact of trench defects in InGaN/GaN light emitting diodes and implications for the "green gap" problem *Appl. Phys. Lett.* **105** 112110
- [5] Monavarian M, Rashidi A and Feezell D 2019 A decade of nonpolar and semipolar III-nitrides: a review of successes and challenges *Phys. Status Solidi a* 216 1800628
- [6] Elsaesser D R, Durniak M T, Bross A S and Wetzel C 2017 Optimizing GaInN/GaN light-emitting diode structures under piezoelectric polarization J. Appl. Phys. 122 115703
- [7] Church S A, Ding B, Mitchell P W, Kappers M J, Frentrup M, Kusch G, Fairclough S M, Wallis D J, Oliver R A and Binks D J 2020 Stacking fault-associated polarized surface-emitted photoluminescence from zincblende InGaN/GaN quantum wells Appl. Phys. Lett. 117 032103
- [8] Church S A, Quinn M, Cooley-Greene K, Ding B, Gundimeda A, Kappers M J, Frentrup M, Wallis D J, Oliver R A and Binks D J 2021 Photoluminescence efficiency of zincblende InGaN/GaN quantum wells J. Appl. Phys. 129 175702
- [9] David A and Grundmann M J 2010 Influence of polarization fields on carrier lifetime and recombination rates in InGaN-based light-emitting diodes *Appl. Phys. Lett.* 97 033501
- [10] Vurgaftman I and Meyer J R 2003 Band parameters for nitrogen-containing semiconductors *J. Appl. Phys.* 94 3675–96
- [11] Binks D J, Dawson P, Oliver R A and Wallis D J 2022 Cubic GaN and InGaN/GaN quantum wells Appl. Phys. Rev. 9 041309
- [12] Frentrup M, Lee L Y, Sahonta S-L, Kappers M J, Massabuau F, Gupta P, Oliver R A, Humphreys C J and Wallis D J 2017 X-ray diffraction analysis of cubic zincblende III-nitrides J. Phys. D: Appl. Phys. 50 433002
- [13] Lee L Y, Frentrup M, Vacek P, Kappers M J, Wallis D J and Oliver R A 2024 Investigation of stacking faults in MOVPE-grown zincblende GaN by XRD and TEM J. Appl. Phys. 125 105303
- [14] Wright A F 1997 Basal-plane stacking faults and polymorphism in AlN, GaN, and InN J. Appl. Phys. 82 5259–61

- [15] Glas F 2008 A simple calculation of energy changes upon stacking fault formation or local crystalline phase transition in semiconductors J. Appl. Phys. 104 093520
- [16] Vacek P, Frentrup M, Lee L Y, Massabuau F C-P, Kappers M J, Wallis D J, Gröger R and Oliver R A 2021 Defect structures in (001) zincblende GaN/3C-SiC nucleation layers J. Appl. Phys. 129 155306
- [17] Ding B, Frentrup M, Fairclough S M, Kappers M J, Jain M, Kovács A, Wallis D J and Oliver R A 2020 Alloy segregation at stacking faults in zincblende GaN heterostructures J. Appl. Phys. 128 145703
- [18] Gundimeda A, Kusch G, Frentrup M, Kappers M J, Wallis D J and Oliver R A 2024 Cathodoluminescence studies of the optical properties of a zincblende InGaN/GaN single quantum well *Nanotechnology* 35 395705
- [19] Lee L Y, Frentrup M, Kappers M J, Oliver R A, Humphreys C J and Wallis D J 2018 Effect of growth temperature and V/III-ratio on the surface morphology of MOVPE-grown cubic zincblende GaN J. Appl. Phys. 124 105302
- [20] Oliver R A et al 2013 The impact of gross well width fluctuations on the efficiency of GaN-based light emitting diodes Appl. Phys. Lett. 103 141114
- [21] Haller C, Carlin J F, Jacopin G, Martin D, Butté R and Grandjean N 2017 Burying non-radiative defects in InGaN underlayer to increase InGaN/GaN quantum well efficiency Appl. Phys. Lett. 111 262101

- [22] Lähnemann J et al 2023 LumiSpy/lumispy: v0.2.2 Zenodo (available at: https://doi.org/10.5281/zenodo.7747350)
- [23] Gundimeda A, *et al* 2024 Impact of stacking faults on the luminescence of a zincblende InGaN/GaN single quantum well *J. Appl. Phys.* **58** 025112
- [24] Church S A *et al* 2017 Photoluminescence studies of cubic GaN epilayers *Phys. Status Solidi b* **254** 1600733
- [25] Wang H, Ji Z, Qu S, Wang G, Jiang Y, Liu B, Xu X and Mino H 2012 Influence of excitation power and temperature on photoluminescence in InGaN/GaN multiple quantum wells Opt. Mater. Express. 20 3932–40
- [26] Alreshidi F et al 2024 Enhanced efficiency InGaN/GaN multiple quantum well structures via strain engineering and ultrathin subwells formed by v-pit sidewalls ACS Appl. Opt. Mater. 2 220–9
- [27] Hammersley S, Kappers M J, Massabuau F C-P, Sahonta S-L, Dawson P, Oliver R A and Humphreys C J 2015 Effects of quantum well growth temperature on the recombination efficiency of InGaN/GaN multiple quantum wells that emit in the green and blue spectral regions *Appl. Phys. Lett.* 107 132106
- [28] Armstrong A M, Bryant B N, Crawford M H, Koleske D D, Lee S R and Jj W Jr 2015 Defect-reduction mechanism for improving radiative efficiency in InGaN/GaN lightemitting diodes using InGaN underlayers J. Appl. Phys. 117 134501